

N 62 13906

# CASE FILE COPY

*Technical Report No. 32-271*

## *Use of Carbon Arc Lamps as Solar Simulation in Environmental Testing*

*J. E. Maclay*

*R. J. Goggia*

FACILITY FORM 602

N62-13906  
(ACCESSION NUMBER)

29  
(PAGES)

JPL-TR-32-27  
(NASA CR OR TMX OR AD NUMBER)

(THRU)

3

(CODE)

10

(CATEGORY)

jpl

JET PROPULSION LABORATORY  
CALIFORNIA INSTITUTE OF TECHNOLOGY  
PASADENA, CALIFORNIA

June 4, 1962


NATIONAL AERONAUTICS AND SPACE ADMINISTRATION  
CONTRACT No. NAS 7-100

*Technical Report No. 32-271*

*Use of Carbon Arc Lamps as Solar Simulation  
in Environmental Testing*

*J. E. Maclay*

*R. J. Goggia*



N. F. Jacobson, Chief  
Program Engineering Section

JET PROPULSION LABORATORY  
CALIFORNIA INSTITUTE OF TECHNOLOGY  
PASADENA, CALIFORNIA

June 4, 1962

Copyright© 1962  
Jet Propulsion Laboratory  
California Institute of Technology

## CONTENTS

<b>I. Introduction</b>	1
<b>II. Criteria for a Space Simulator</b>	1
<b>III. Background Information for Solar Simulation</b>	4
A. Sources Considered for Solar Simulation	4
B. Possible Optical Systems	4
C. Geometry of the Chamber to be Used	5
D. Spatial Distribution of a Bare Lamp	6
E. Radiant Power Output of a Bare Lamp	6
F. Spectral Intensity Distribution of a Bare Lamp	6
<b>IV. Possible Optical Systems to Adapt Carbon Arc Lamp to     Solar Simulator</b>	8
<b>V. Conclusion</b>	10
<b>Appendixes</b>	
A. Comparison of Radiative Heat Transfer in the Space Simulator and in Free Space	11
B. Comparison of Conductive and Radiative Heat Transfer in the Space Simulator	12
C. Temperature of a Spacecraft	13
D. Measurement of Spatial Light-Intensity Distribution	15
E. Measurement of Radiant Heat-Power Output	16
F. Measurement of Spectral Intensity Distribution	18
G. Design of a Projection-Type Optical System for the Solar Simulator	21
H. Design of the Long Focal-Length Lens Optical System and Sunflower	23
<b>References</b>	25

## TABLES

1. Comparison of surface absorptions for different materials and radiation sources . . . . .	3
2. Radiant power output for various apertures . . . . .	6
B-1. Comparison of radiative and conductive heat transfer in a space simulator . . . . .	12
E-1. A sample calculation of arc-lamp power for a typical situation . . . .	16
E-2. Wattage values using several different pulse durations . . . . .	16
E-3. Effect on measured wattage values of high initial calorimeter temperature . . . . .	17
E-4. Lamp power output as a function of feed rate and current . . . . .	17
E-5. Power output from front- and rear-surface mirrors . . . . .	17

## FIGURES

1. View of opened vacuum chamber showing floor and wall shrouds for liquid nitrogen . . . . .	5
2. View of arc lamps in position over closed vacuum chamber . . . . .	5
3. Differences in spatial distribution of the bare arc lamp caused by changes in mirror position . . . . .	6
4. Differences in spectral distribution of the bare arc lamp caused by changes in mirror position . . . . .	7
5. Differences in spectral distribution caused by front- and rear-surfaced mirrors . . . . .	7
6. Spectral distribution of the bare arc lamp . . . . .	7
7. Typical spatial distribution of the arc lamp with a prismatic lens . . . .	8
8. Typical spatial distribution of the arc lamp with a long focal length lens . . . . .	8
9. Spatial distribution across the payload using an arc lamp with long focal length lens, ground Vycor, and sunflower . . . . .	9
10. Comparison of spectral distribution of arc lamp and solar radiation . . . . .	9
D-1. Position of detector for spatial intensity measurements . . . . .	15
D-2. Detector plane in spacecraft orientation . . . . .	15
F-1. Block diagram of a spectroradiometer . . . . .	18
F-2. Schematic of spectroradiometer optical system . . . . .	19
G-1. Light pattern on spacecraft in 6-ft solar simulator . . . . .	21
H-1. Blades typical of those used on the sunflower . . . . .	23
H-2. Typical spatial distribution ( $I_p$ ) and its transmittance curve ( $T_p$ ) . . . .	24

## ABSTRACT

This report covers work done by the authors on the solar simulator for the six-foot diameter space simulator presently in use at JPL. The space simulator was made by modifying an existent vacuum chamber and uses carbon arc lamps for solar simulation. All *Ranger* vehicles flown to date have been tested in this facility.

The report also contains a series of appendixes covering various aspects of space-simulation design and use. Some of these appendixes contain detailed analyses of space-simulator design criteria. Others cover the techniques used in studying carbon-arc lamps and in applying them as solar simulation.

## I. INTRODUCTION

This report describes work performed in 1959 and 1960 on the solar simulator to be used on the 6-ft  $\times$  7-ft space simulator presently located at JPL. Other features of a space simulator are mentioned but only to establish a proper frame of reference for treating solar simulation problems. It is assumed that the reader has

an appreciation for the role of a space simulator in environmental testing, and no attempt to "sell" space simulator testing will be made. The body of the report concerns the simulator proper, and a collection of eight appendixes cover various aspects of the design of that simulator.

## II. CRITERIA FOR A SPACE SIMULATOR

To duplicate free space would be extremely difficult if not impossible. A criteria must be established to set limits on how closely free space must be duplicated in order that the payload under test perform the way it would in free space.

There are three prominent features of free space: (a) an almost  $4\pi$  steradian radiation background at about 4° K, (b) a pressure of about  $10^{-17}$  mm Hg, and (c) a solar radiation which is infinitely uniform, collimated to  $\pm 1/4$  deg, and has an intensity which varies inversely

with the square of the solar distance. There are other features such as planetary background sources, cosmic radiation and other phenomena, but these are second order (or less) effects in the thermal problem; hence, they will not be considered in this report. Because this report is concerned with the utilization of carbon arc sources as a solar simulator, neither the radiation background nor the pressure will be dwelt on extensively.

The radiative heat transfer between two concentric bodies has two aspects which need investigation. The interchange is proportional to the difference of the temperatures raised to the fourth power and also to a form factor which is dependent on area, geometry, and emissivity.

The degree of simulation achieved by the space simulator with respect to background temperature is easily shown by comparing the quantities  $(T_{sc}^4 - T_{bg}^4)$  for free space conditions and space simulator conditions, where  $T_{sc}$  is the spacecraft temperature and  $T_{bg}$  is the background temperature. It is shown in Appendix A that the difference between these quantities for free space and for a space simulator at liquid nitrogen temperature (80° K) is only one part in 210 (assuming a spacecraft at 25° C); therefore, the liquid nitrogen background simulates free space quite well.

The form factor is also easily assessed. The radiation interchange between two concentric bodies is proportional to

$$\frac{1}{\frac{1}{\epsilon_{sc}} + \frac{1}{\epsilon_{bg}} - 1}$$

where  $\epsilon_{sc}$  and  $\epsilon_{bg}$  are the emissivities of the spacecraft and background, respectively (see Appendix A). If the inner body is small compared to the outer (as in free space), the expression reduces to  $\epsilon_{sc}$ . The degree of simulation achieved by the space simulator with respect to this second factor is shown by comparing the aforementioned quantities. In Appendix A it is shown that for a typical range of spacecraft emittances in the space simulator concerned in this report, the quantities for free space and space simulator conditions differ by 2 to 5 parts per hundred. (This form factor is based on the assumption that the background covers a  $4\pi$  solid angle. In Appendix A it is shown that for free space, the background covers almost  $4\pi$  steradians and the background of the space simulator as presently built covers  $3.9\pi$  steradians, a difference from free space of only 1 part in 40.)

The low pressure of free space effectively eliminates thermal conductivity through gas. It is clearly impossible to reproduce the free space pressure, but it is shown in Appendix B that at a pressure of  $10^{-6}$  mm Hg or less, the heat transfer through gas within the spacecraft and between the spacecraft and the space simulator is negligible compared to the radiative heat transfer; hence,  $10^{-6}$  mm Hg is an adequately low pressure for the simulation of space.

The solar radiation is the most critical feature of free space, and it is one in which technology lags the present needs. It was shown that the radiation background and pressure conditions of free space were easily simulated to a satisfactory degree by the current technology. The balance of this report will be concerned with solar simulation.

Solar radiation has four critical facets which must be viewed independently when establishing solar simulation criteria, as each of the four has a definite effect.

The sun is a spherical radiator, hence, at the distance of the planets it can be regarded as having an infinitely uniform flux distribution over any conceivable spacecraft. Recalling that the solar heat input to a unit area is given by  $I_s \alpha$ , the product of solar intensity and solar absorption of the surface, it is easily seen that if the solar simulator has non-uniform intensity, then different locations on a surface will have different heat inputs. This would establish thermal gradients in that surface which are not identical to those formed under free space conditions. The criteria here is not easily established; it is a function of the item being tested in the space simulator. If the intensity irregularities are small and random and the spacecraft surface has a good thermal conductivity, then these gradients would average out. If the flux irregularities are of a size comparable to the spacecraft, or if the intensity differences are great, then even an extremely high thermal conductivity of the surface will not average out the flaws, and unspacelike conditions will exist in the spacecraft. Even so, if these solar simulator-induced temperature differences are small compared with the differences established by internal power dissipations then the degree of simulation is still satisfactory. In lieu of a more precise criteria, the degree of simulation required with regard to flux uniformity must be as good as the technology will allow and even then its interaction with the spacecraft must be evaluated.

Solar radiation is, for thermal purposes, perfectly collimated (i.e., 100% of the energy is within a cone of  $\frac{1}{4}$

deg half-angle). The effect of non-collimated radiation is to distort shadows which the portions of the spacecraft facing toward the sun cast on those portions below, thereby affecting the solar heat input. Again, the degree of simulation required is a function of the item under test. A small discrepancy in shadow size on a large surface may be negligible whereas the same discrepancy on a small surface could be serious. It was established that for *Ranger* and *Mariner* Program spacecraft, a collimation of  $\pm 6$  deg would be adequate inasmuch as this limits the distortion of shadow dimensions to less than one tenth the distance from the shadowing object to the shadow. Both flux uniformity and collimation are to a great extent functions of the optics employed in the solar simulator and may be fairly independent of the radiation energy source.

The intensity of solar radiation in space is dependent upon the distance from the sun, following an inverse square relationship. The intensity varies from 58.27 mw/cm<sup>2</sup> at Mars to 135 mw/cm<sup>2</sup> at Earth to 258.7 mw/cm<sup>2</sup> at Venus. Recalling the equation governing the thermal conditions of an isolated body (Appendix C), the equilibrium temperature is, among other things, proportional to the  $+1/4$  power of the solar intensity. Once again, however, this effect is dependent upon the particular spacecraft because a large internal power dissipation could make this a minor effect. On the other hand, this facet of the solar simulator is the easiest to control. It is basically a function of source output, but can be modified by introducing aperture stops or neutral-density filters into the optics.

The spectral distribution of the solar simulator is also a critical characteristic and an elusive one. It can be seen why it is critical by its effect on the solar absorption of a surface (Appendix C). If a solar absorption for a surface is calculated using the formula,  $\alpha = \frac{\int \alpha(\lambda) s(\lambda) d\lambda}{\int \alpha(\lambda) d\lambda}$ , first with  $s(\lambda)$  being a solar spectral distribution and then letting  $s(\lambda)$  be any other source spectral distribution, the two values of  $\alpha$  will, in general, be different because  $\alpha(\lambda)$  is strongly wavelength dependent

for most surfaces. This, in turn, affects the equilibrium temperature. As an example, the absorptions of three surfaces were calculated for: solar input,  $\alpha_s$ ; Hg-Xe arc lamp input,  $\alpha_{\text{Hg-Xe}}$ ; and a carbon-arc lamp input,  $\alpha_c$  (see Table 1). All three surfaces are representative of those used in the current spacecraft series.

**Table 1. Comparison of surface absorptions for different materials and radiation sources**

	$\alpha_s$	$\alpha_{\text{Hg-Xe}}$	$\alpha_c$	$\frac{\Delta\alpha_{\text{Hg-Xe}}}{\alpha_s}$	$\frac{\Delta\alpha_c}{\alpha_s}$
White paint	0.22	0.29	0.20	32%	9%
Grit blasted aluminum	0.46	0.48	0.46	4%	0%
Gold plated magnesium	0.28	0.30	0.26	7%	7%

It is clearly seen that the criteria for simulation depends on the item to be tested. Notice that the spectral intensity distribution can also cause troubles which will appear to be due to flux non-conformity if a spacecraft has more than one surface material. The spectral distribution of a solar simulator is basically a matter of energy source selection; at the power levels involved in a space simulator, selective filters are of little or no use due to the magnitude of the energy absorbed by those filters. To compound the problem: although the bulk of the solar radiation spectrum has been measured, the ultraviolet energy and thus its effect on the thermal problem is less well defined.

Throughout this discussion of the solar simulation criteria, the recurrent theme has been that the degree of simulation required is dependent upon the item to be tested in the space simulator. Deep space radiation background and deep space pressure are easily simulated with the present day technology for any conceivable spacecraft, but solar simulation must await significant advances, before the same can be said of it.



### III. BACKGROUND INFORMATION FOR SOLAR SIMULATION

#### A. Sources Considered for Solar Simulation

The solar radiation at the Earth's surface is not a good substitute for solar radiation in space for several reasons. The UV component is missing due to atmospheric absorption. The intensity level is reduced to about 75% of that outside the atmosphere. Lastly, the Sun does not provide the continuously operating source necessary for long tests.

An artificial solar source should fulfill the criteria mentioned in Section II and also some others. It must be suitable for days of reliable operation and must have a geometrical radiation pattern such that it will be compatible with an optical system which can project the radiation as parallel light over the testing area. To be compatible with the rest of a simulated deep-space environment, the source may have to operate in a vacuum, depending upon the optical system used.

Naturally, no perfect source was found. Some possible sources eliminated themselves. Tungsten lamps have a spectral distribution which was far from that of solar radiation. The new short-arc mercury vapor and xenon lamps were rejected because of low power level, unsuitable geometrical radiation patterns, and inability to operate horizontally or in a vacuum. (Since the time that this selection work was performed, the technology in short-arc vapor lamps has been advanced significantly.) The feasibility of plasmotrons was not obvious, and one plasmatron vendor felt that it would require a year of intensive research to determine whether they could be used.

This left only carbon arc lamps, which could be used external to the vacuum only. Because large windows in a vacuum chamber are not feasible, it also meant that parallel light would be difficult to obtain without very complex optics. On the positive side were two very important points. Vendor data indicated that the spectral distribution of a carbon arc matched that of the Sun quite closely; however, this remained to be proven. In addition, carbon arc lamps were said to be capable of enormous radiant energy levels because the input power to radiant power conversion efficiency is 50 to 60%; this also remained to be proven.

The National Ventarc carbon arc lamp was selected. It is a theater-type projector lamp operating at 155 amps,

75 volts. The position of the arc is held at one focus of an ellipsoidal mirror by an electro-optical servo system. The arc is stabilized by a magnetic field and can operate in any position by virtue of a forced air jet which removes exhaust products independently of gravity or natural convection. As will be shown later, the ellipsoidal mirror was necessary to satisfy another consideration. This was the most powerful lamp available with the ellipsoidal mirror feature. The solar simulator was designed with four lamps so that they could be operated in pairs, one pair being serviced (change carbon rods) while the others are operated. This would permit round-the-clock operation.

#### B. Possible Optical Systems

The possible optical systems fall into two categories; those which transform the radiation from the source into collimated radiation, and those which do not.

Of the former, the Cassegrainian system is perhaps the simplest. A source placed (or imaged by another optical element) at the focus of a parabolic mirror results in collimated radiation after reflection. For our purposes, such a system had many drawbacks. The large mirror would destroy much of the low temperature radiation background, unless cooled. (Even if the mirror were cooled,  $\epsilon$  would remain low; see Appendix A for the importance of high  $\epsilon$ .) The output of more than one arc lamp is needed to give the intensity level desired, and it would be difficult to image two or more distinct sources precisely at the focus of the paraboloid. The intensity of the collimated beam is not uniform: it varies as the inverse square of the distance traveled by the ray between the source and the point on the mirror from which it was reflected. Finally, obtaining a parabolic mirror of suitable dimensions would be no mean task. Reflectors from government surplus searchlights have a very short focal length compared to the diameter ( $f/4$ ), so that the intensity at the edge would be about one-half that at the center. Another point, more subtle, was that with the existing vacuum chamber (described later) the spacecraft would be so near the mirror that its radiation would reflect back upon itself. All things considered, the parabolic mirror method did not seem feasible. Refracting systems were physically out of the question, due to the large diameters.

The non-collimated systems are those in which divergent radiation falls on the spacecraft, and are inherently more simple than others. Disadvantages are the shadow effect mentioned earlier and vertical variations in intensity. Advantages are that multiple sources are no problem, small entrance openings are sufficient, and the simplicity would be more compatible with the time schedule. Consequently, a divergent scheme was deemed to be the most practical approach.

The divergent light from each lamp could cover its portion of the spacecraft, or light from each could cover the entire spacecraft, overlapping. To permit continuous operation (the carbon arc lamps require servicing every 22 minutes), it was necessary to overlap the beams.

### C. Geometry of the Chamber to be Used

The vacuum chamber to be utilized as the space simulator has been at JPL for some time. It is a steel chamber of 6-ft inside diameter and 9-ft inside maximum height, the cylindrical section being 7 ft high. The chamber is built in a corner of the building and, opening vertically, has vertical guide rails. The geometry of the installation placed severe physical constraints on the solar simulator. The size of the lamphouses dictated a minimum possible bolt circle on which the entrance ports were to be mounted, and the necessity of removing the lamps before raising the bell jar dictated the maximum envelope available for the solar simulator. The net result was that the lamps were located so that their optical axes did not intersect the spacecraft at the center, and the radiation patterns, therefore, do not exactly overlap. The completed space simulator is shown in Figs. 1 and 2.

To provide the space background, the chamber walls were lined with a barrel section fabricated of panels made by seam-welding a sheet of corrugated stainless steel to a steel sheet, with the ends suitably manifolded. Liquid nitrogen enters at the bottom and is vented at the top. The top and bottom are lined with shrouds fabricated from spherical stainless steel segments. The upper shroud has portholes to match the entrance ports in the chamber, and both upper and lower shrouds have independent liquid nitrogen circuits. The shrouding is painted with black lacquer on the inside ( $\epsilon > 0.90$ ) and electropolished on the outer surface. The chamber can be pumped down to  $2 \cdot 10^{-6}$  mm Hg, with a typical spacecraft inside, by means of a mechanical pump and a 17-in. oil diffusion pump.

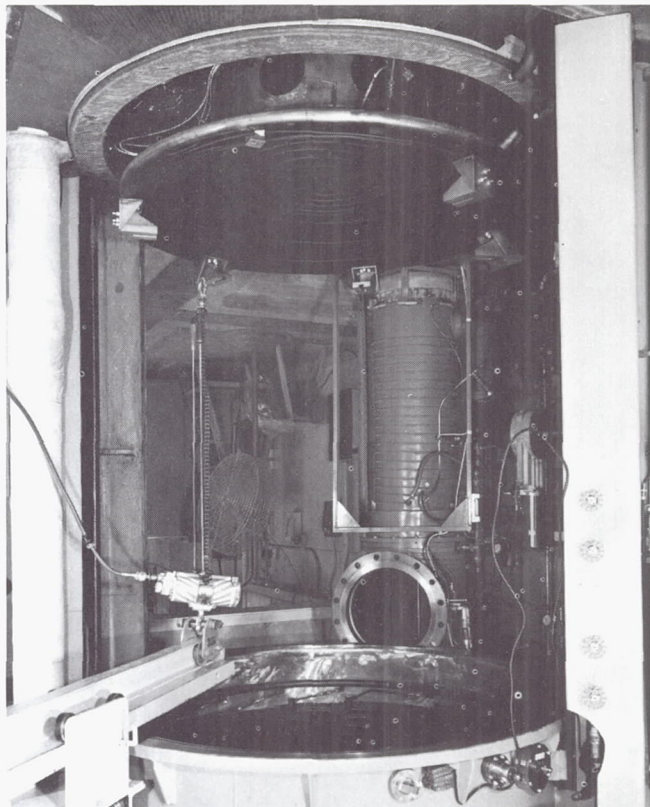


Fig. 1. View of opened vacuum chamber showing floor and wall shrouds for liquid nitrogen

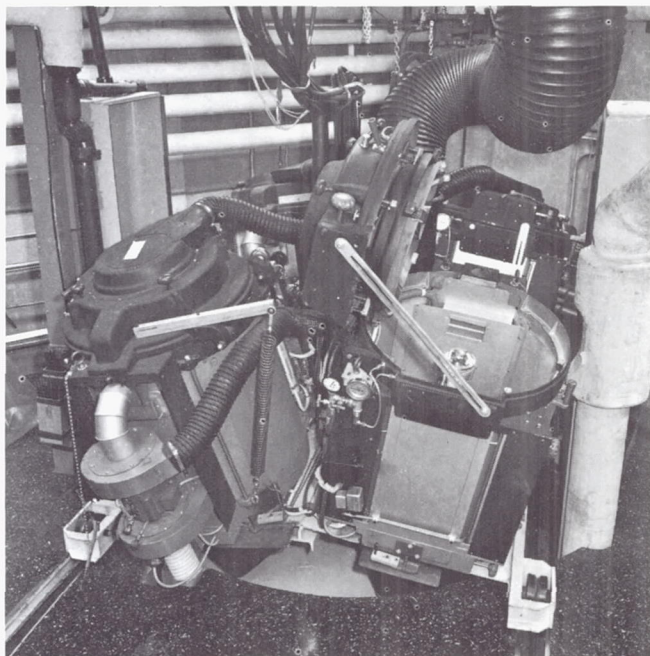


Fig. 2. View of arc lamps in position over closed vacuum chamber



### D. Spatial Distribution of Bare Lamp

The radiation from the lamp with no projection lens is contained in a cone of 16-deg half angle. The pattern from a bare lamp has a doughnut shaped distribution, a shadow in the center, and odd patterns of scattered light from the lamp-house walls around the edge. (See Appendix D for technique of spatial distribution measurement.) Further, the doughnut is lopsided; i.e., the beam is not rotationally symmetric. This is due to the fact that the hole in the ellipsoidal mirror is not centered but is displaced to accommodate an unsymmetrical electrode holder. The mirrors themselves are "sagged" mirrors. A glass sheet is heated and allowed to sag down into a hot mold. The surfaces are then flame-polished and silvered on the rear surface. [In defense of the lamps, it must be said that for their intended purpose (the theater), these flaws were immaterial.]

During the early stages, the importance of the relative positions of the arc and the ellipsoidal mirror was not fully understood, so the spatial distribution was measured with three different relative positions; the arc too far from the mirror, too close to the mirror, and approximately at the focus of the mirror. These results are shown in Fig. 3.

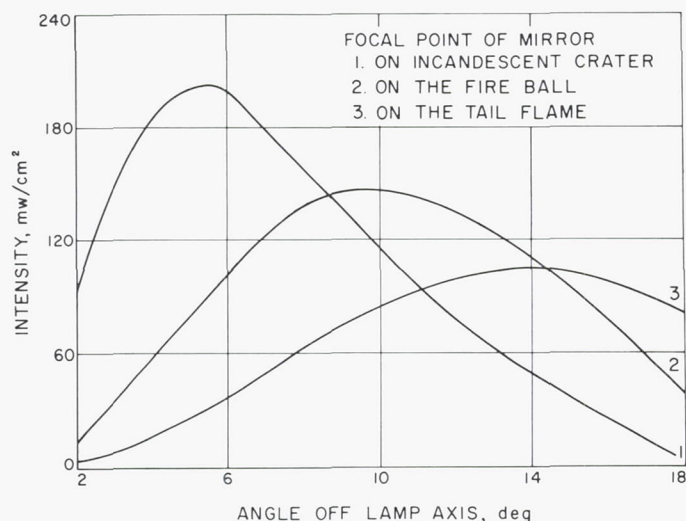


Fig. 3. Differences in spatial distribution of the bare arc lamp caused by changes in mirror position

### E. Radiant Power Output of Bare Lamp

The only figures available for radiant power output of the Ventarc lamp were made with a rear surface mirror and through a 35-mm film aperture with the arc burning at 150-155 amps; i.e., a typical theater installation. Inasmuch as it was thought to be necessary to vary these

three parameters (current, aperture, and mirror surface) to alter the spectral distribution and intensity, it was necessary to find the radiant power dependence on these parameters. Later, during a different type of measurement, it was discovered (and confirmed by the manufacturer) that the arc has a very narrow current range in which it burns stably. Hence, this parameter is not available for control.

The power output through various apertures is given in Table 2 (see Appendix E). Using a front-surface mirror increases output 32% over that with a back-surface mirror.

Table 2. Radiant power output for various apertures

Aperture, in.	Power, w	$\sigma^a$
3	2348	134
2½	1780	106
2¼	1478	73
2	1323	102
1¾	1028	47
1½	791	38
1¼	743	38

<sup>a</sup> Standard deviation.

### F. Spectral Intensity Distribution of a Bare Lamp

The spectral distribution of an arc lamp with an ellipsoidal mirror is variable over a wide range. The mirror may focus the blue tail flame on the payload or the red incandescent crater walls but it is the fire-ball between these extremes which is important. The current range for a stable arc with a given rod is so narrow, less than 10 amps, that current cannot be used as a control parameter for spectral distribution or radiant power control. This point is mentioned because the original conception was just the reverse; i.e., that focusing was unimportant to spectral distribution and that current control would be the variable. This is shown by Fig. 4. The spectral distribution was measured (see Appendix F) for the same three relative positions of arc and mirror that were used when spatial intensity was measured (see Section III D). These measurements were hurriedly performed, and are only intended to show color changes. In Fig. 5 the color difference for a front-surface mirror and a back-surface mirror are shown. The mirror position was changed by the mirror thickness so that the reflecting surface remained in the same position. This work also was performed hurriedly, only to show the color shift. Figure 6

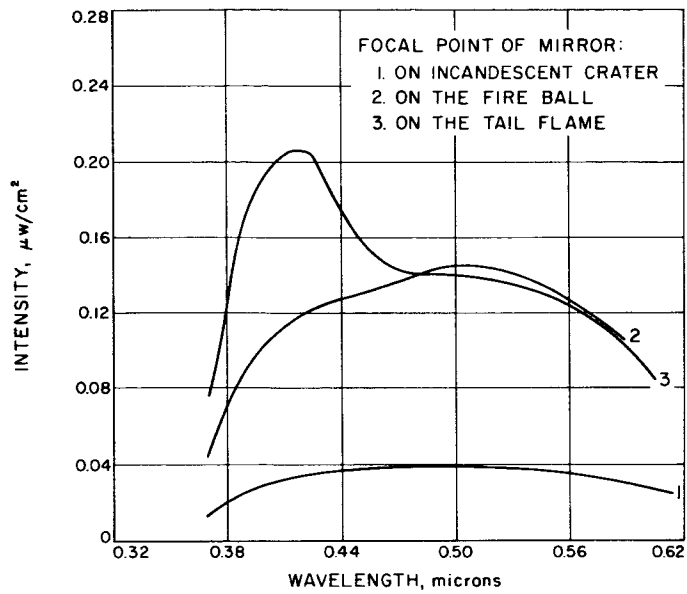


**Fig. 4. Differences in spectral distribution of the bare arc lamp caused by changes in mirror position**

shows the carefully measured spectral distribution of an arc located at the focus of a front-surface mirror (about

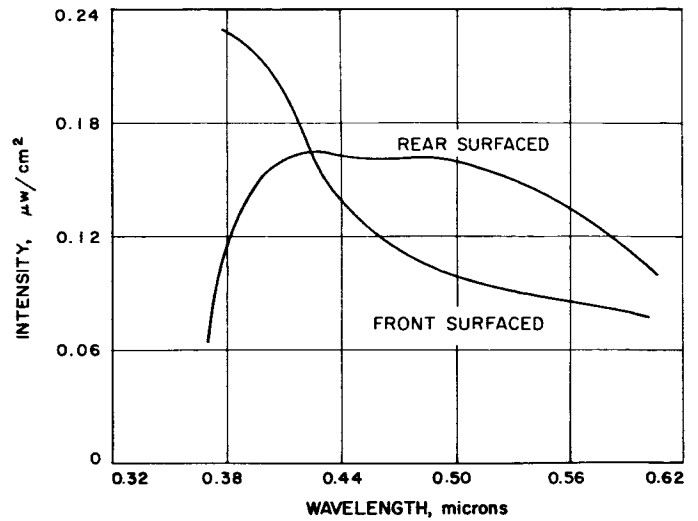


**Fig. 5. Differences in spectral distribution caused by front- and rear-surfaced mirrors**

8 deg off axis) with no optical system. Other measurements (not illustrated) showed that there are small (a matter of inches) zonal irregularities in the beam, with regard both to color and intensity.

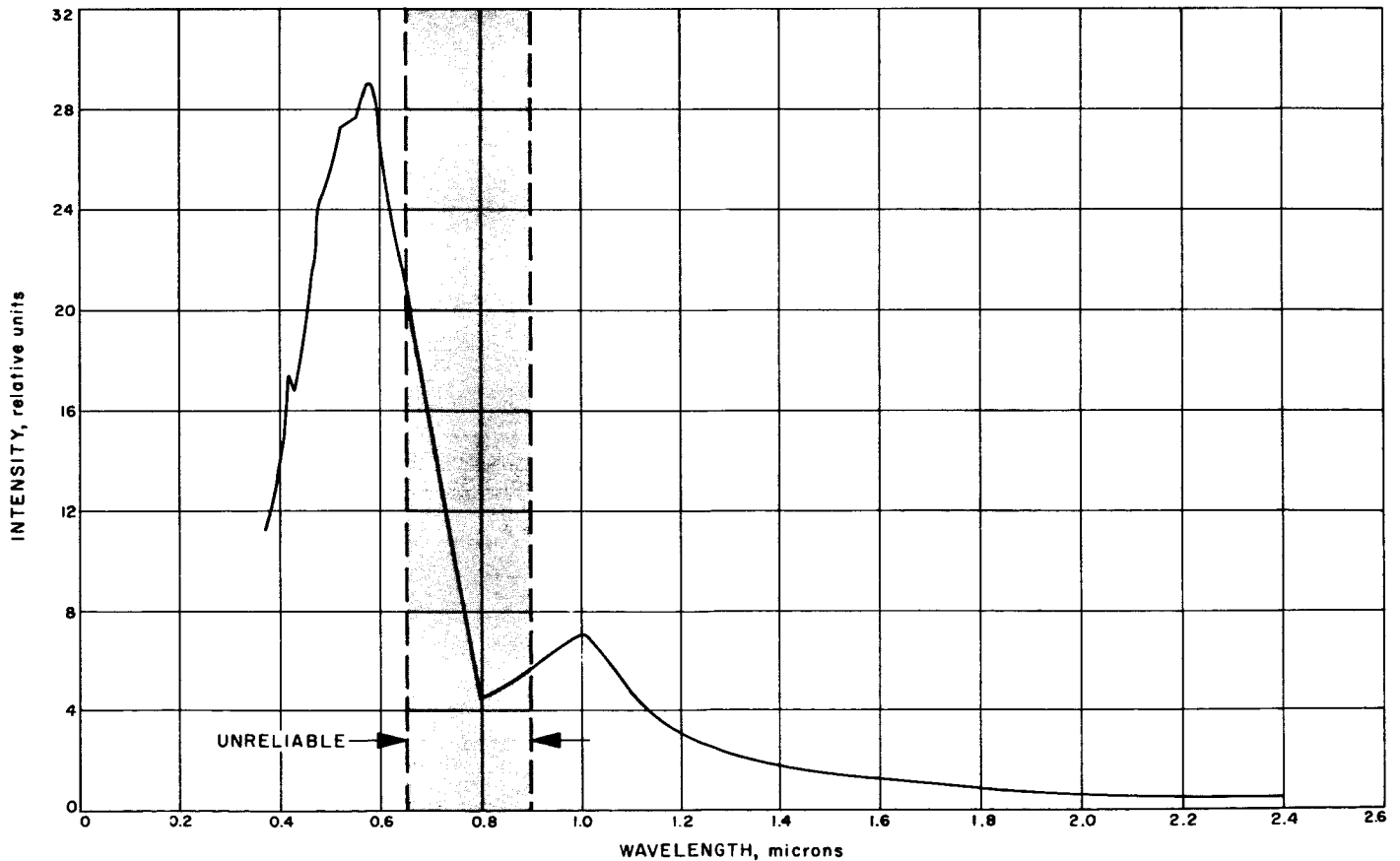


**Fig. 6. Spectral distribution of the bare arc lamp**

#### IV. POSSIBLE OPTICAL SYSTEMS TO ADAPT CARBON ARC LAMP TO SOLAR SIMULATOR

Based on the knowledge gained from studies of the bare lamp and constrained by vacuum chamber configuration and the impracticality of collimation, a suitable optical system was developed. Although only two systems were explored in detail, several were considered and immediately rejected.

In theater use, a projection lens focuses the fireball image (second focus of ellipsoidal mirror) on the screen, appropriately modified by the film, of course. It is important to note that there is no dark spot in the center of the screen corresponding to the hole in the ellipsoidal mirror; this is because the hole in the mirror is out of focus. This fire-ball is imaged on a screen whose distance is much greater than its dimensions.

The first system to be considered was an adaptation of a theater system capable of imaging the fire-ball on the spacecraft. The method for the design of this system is indicated in Appendix G. The system tried was not designed analytically, but by trial-and-error, using a number of different lenses because, as pointed out in Appendix G, the problem is no longer in the realm of thin-lens approximations. This particular system also employed a prism to relieve some of the physical constraints on lamphouse mounting by bending the lamp axis. This system was not successful in use although it worked well on the bench with a light bulb as a source. Appendix G shows why: this system is sensitive to changes in the position of the arc, and this effect was quite pronounced in use. The spatial distribution for this system mounted on an arc lamp is shown in Fig. 7.

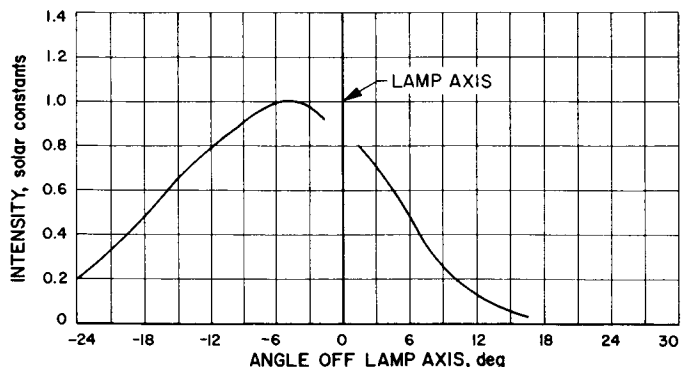


Fig. 7. Typical spatial distribution of the arc lamp with a prismatic lens

Rotation of the prism (not illustrated) had no marked effect on the spatial distribution.

The second system considered was a lens to focus the ellipsoidal lamphouse mirror on the spacecraft. The spacecraft would then be as uniformly irradiated as the mirror, which meant a drop-off at the outer edge and a shadow in the center. The design of this system is discussed in Appendix H. This system has two good points, in spite of other shortcomings. The lens has a long focal length, so that it is not sensitive to arc position. For the same reason, the position of the lens itself is not critical, so that it is compatible with simple, durable mounts and operation by personnel who are relatively unfamiliar with optical systems. These two advantages have been borne out in practice. The spatial distribution of an arc lamp with this system is shown in Fig. 8. This data was taken with the lamp and measuring device in the same configuration as the lamp and spacecraft have during a space simulator test (see Appendix D).

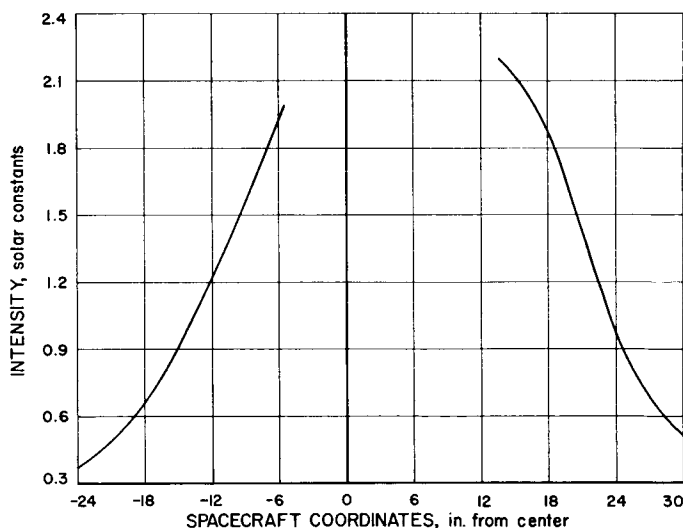


Fig. 8. Typical spatial distribution of the arc lamp with a long focal length lens

In actual use, another modification was introduced into the system to flatten the spatial distribution. Because of the ample intensity level in the center of the spacecraft, it was possible to selectively attenuate the central portions of the beam and bring it all down to the same moderate level. An attempt was made to flatten the

spatial distribution solely by diffusers but the results were discouraging because the overall intensity was reduced without any appreciable flattening. The desired effect was achieved by placing a sunflower shaped scrim in the beam, together with a sheet of ground Vycor to diffuse the sunflower's shadow. The design of this sunflower is covered in Appendix H. The spatial distribution of an arc lamp with the long focal length lens, sunflower, and diffuser is given in Fig. 9. Again, the lamp and measuring device were in a space simulator configuration. The intensity is lower than expected, due to the diffuser. The diffuser cut the intensity to about half because of back reflection. It should be pointed out that with the high thermal conductivity of the spacecraft surface, the sunflower shadow might not matter, but it would have been impossible to measure the average intensity with a small-target detector. The diffuser further helped at the edges of the spacecraft by scattering light out from the center. The selection of grind on the diffuser was entirely by trial and error.

The spectral distribution of this system was measured primarily to find if the spacecraft irradiation was of a

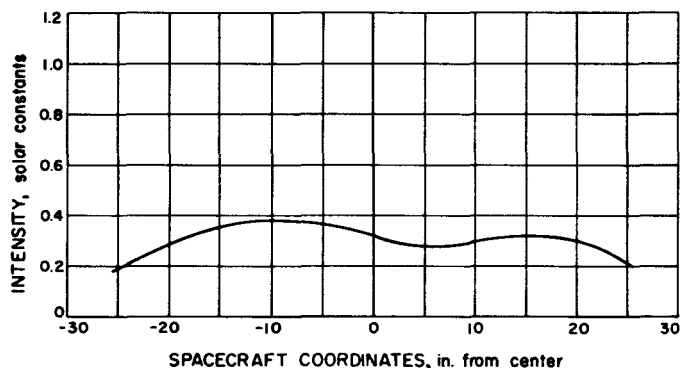


Fig. 9. Spatial distribution across the payload using an arc lamp with long focal length lens, ground Vycor, and sunflower

uniform color-temperature. Due in large part to the diffuser, there were no signs of any color change out to the position corresponding to the edge of the spacecraft. This distribution (for only one position in the irradiation pattern) is shown in Fig. 10 plotted against a solar spectral distribution of equal energy. Note that the ellipsoidal mirror needed a slight re-adjustment to bring more blue tail flame into focus. No total power output measurement was ever performed on this system since such a measurement is really of little value.

Other systems were considered, but not tried. Although an integrating sphere has a very uniform illumination field, it is a very inefficient transfer system (as our trial unit proved) and the method was dropped. A light pipe was considered, but the idea was abandoned because of prohibitive absorption losses.

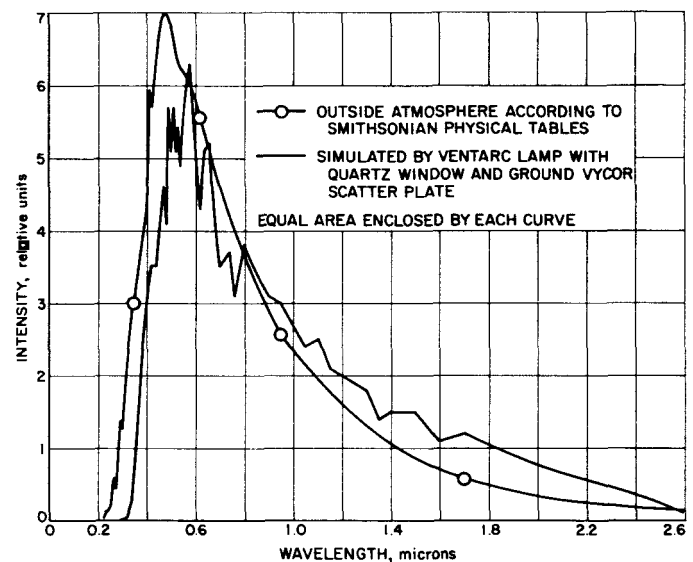


Fig. 10. Comparison of spectral distribution of arc lamp and solar radiation

## V. CONCLUSION

Under the circumstances, it is felt that the sunflower system was the best choice. Many firm boundary conditions, such as vacuum chamber dimensions and location, and time and money restrictions, coupled together with an underestimation of the magnitude of the job, are all part of the circumstances which influenced the choice. The sunflower system has proven to be stable during days of testing and requires a minimum of operator attention. The optical elements require occasional cleaning (every 4 hours, or so), but are easily replaced because the position of the elements is not critical. The successful space-simulator testing of *Ranger* Program spacecraft is evidence that although the choice was not the best, it was at least a workable choice. With different boundary conditions, especially those connected with the vacuum chamber, a different optical system would certainly be chosen.

Although the initial performance of the solar simulator was as expected, it later degraded appreciably. The re-

sults of the *Ranger 1* tests could not be correlated with the conditions thought to exist inside the simulator. A measurement of intensity distribution on the spacecraft indicated that the uniformity of the intensity had degraded. Several elements of the solar simulator had aged (Vycor lens turned purple, mirrors pitted), but their replacement did not correct the distribution. The decrease in intensity was identical for all four lamps; it was independent of optical element aging, and it did not change further during the subsequent six months. It was then discovered that the current-control system on the lamps had degraded due to vertical operation; repair and relocation of components brought the solar simulator back to the original performance.

In summary, the space simulator is in existence, and it is being used at this time. The illumination system does not simulate sunlight satisfactorily and corrections to test results must be made, but it is usable.

## APPENDIX A

## Comparison of Radiative Heat Transfer in the Space Simulator and in Free Space

For two concentric bodies of comparable size, the radiative heat transfer between them is given by the equation:

$$q = \frac{\sigma A_1 (T_1^4 - T_2^4)}{\frac{1}{\epsilon_1} + \frac{1}{\epsilon_2} - 1} \quad (\text{A-1})$$

where:

$T_1$  and  $T_2$  = temperature of inner and outer body, respectively

$\epsilon_1$  and  $\epsilon_2$  = emittance of inner and outer body, respectively

$A_1$  = area of inner body, and

$\sigma$  = Stefan-Boltzman constant.

If the inner body is much smaller than the outer, it reduces to:

$$q = \epsilon_1 A_1 \sigma (T_1^4 - T_2^4) \quad (\text{A-2})$$

It will be convenient to evaluate the heat transfer in two steps; first the temperature dependence and second, the emittance term dependence.

In free space, with  $T_2 \cong 4^\circ \text{K}$  and a typical spacecraft temperature of  $30^\circ \text{C}$ , the quantity is  $(303^4 - 4^4) = (84 \cdot 10^8 - 256) \cong 84 \cdot 10^8$ . In the space simulator, with the walls at  $\text{LN}_2$  temperature ( $80^\circ \text{K}$ ), this quantity is  $(84 \cdot 10^8 - 80^4) = (84 - 0.41) \cdot 10^8$ ; that is, the space simulator temperature term differs from that of free space but only .4 parts in 84, or 1 part in 210. This presents an insignificant error.

For the space simulator, the first heat transfer equation (Eq. A-1) is appropriate; for free space, the latter (Eq. A-2). A typical range of values for spacecraft emittance would be  $\epsilon_1 = 0.2$  to  $0.4$ , and for space simulator walls,  $\epsilon_2 = 0.9$ . For free space then, the emittance term is  $0.2$  to  $0.4$ , and in a space simulator, it is

$$\frac{1}{\epsilon + \left( \frac{1}{0.9} - 1 \right)}$$

or  $0.196$  to  $0.383$  for corresponding values of spacecraft emittance. For  $\epsilon_1 = 0.2$ , the error is  $0.004$  in  $0.200$ , or 1 part in 50, an insignificant amount (considering other systematic errors such as non-uniform irradiation); for  $\epsilon_1 = 0.4$ , the error is  $0.02$  in  $0.40$ , or 1 part in 20. This error is of a magnitude such that corrections in the data should be made to offset it.

A last subtle point is that the heat transfer equation is based on the outer body being a full sphere, or subtending  $4\pi$  steradians of solid angle. In free space, the radiation background subtends  $4\pi$  minus the solid angle of the Sun where the Sun subtends  $(0^\circ 32'/180^\circ)^2 \pi = (8.7 \times 10^{-5}) \pi$  steradians. The difference is insignificant, about 1 part in 50,000. In the space simulator the four openings for entrance ports each have a 15-in. diameter at a distance of about 48 in. from the nearest point on the spacecraft. Their individual solid angles will be  $\pi (7.5/48)^2 = 0.024 \pi$  steradians. For the total of four openings, the difference is  $(4\pi - 0.1\pi)$  versus  $4\pi$ . This error of  $0.1$  in  $4$ , or 1 part in 40, is felt to be small enough that the equation for heat transfer is still applicable.



## APPENDIX B

## Comparison of Conductive and Radiative Heat Transfer in the Space Simulator

When operating the spacecraft in the space simulator the question arises: is the equilibrium temperature of the spacecraft a function of radiative mechanisms only, as in free space, or does heat transfer through the rarified gas affect the equilibrium temperature? The latter would have two effects: first, it would mask potential hot spots within the spacecraft by allowing conductive and/or convective cooling, and second, the spacecraft would be cooled by conductive and/or convective heat transfer to the low temperature radiation background.

Convective heat transfer disappears when the pressure is such that the mean-free-path of the gas molecules is comparable with chamber dimensions. In this condition, the gas molecules travel directly from a high temperature surface to the lower, rather than slowly drifting over due to multiple molecular collisions. The mean-free-path of air is given approximately by  $L = 5 \cdot 10^{-3} / P_{mm}$  cm (Ref. 1), and at  $10^{-4}$  mm Hg, the mean-free-path, 50 cm, is comparable with chamber dimensions. Since it will be shown later that the pressure must be even lower yet, it will be assumed that there is no convective heat transfer, only conductive and radiative.

Free molecule conductivity through a gas at low pressure is given by the equation (Ref. 2):

$$E = P_{mm} (0.243) \frac{\alpha}{M^{1/2}} \cdot \frac{T_s - T_i}{T_i^{1/2}} \cdot \frac{\gamma + 1}{\gamma - 1}$$

where

$E$  = conductive heat transfer at low gas pressure, w/cm<sup>2</sup>

$P_{mm}$  = gas pressure, mm Hg

$M$  = molecular weight of gas

$T_s$  = temperature of heat source, °K

$T_i$  = temperature of heat sink, °K

$\alpha$  = "accommodation coefficient," a quantity which accounts for a gas molecule's not coming up to a surface's temperature in one collision; it is a function of surface finish and type of gas

$\gamma$  = ratio of specific heat of the gas at constant pressure to that at constant volume

Radiative heat transfer is governed by the equation (Ref. 3):

$$Q = \epsilon_{s-i} \sigma (T_s^4 - T_i^4)$$

where:

$Q$  = radiative heat transfer, w/cm<sup>2</sup>

$\epsilon_{s-i}$  = "interchange factor," a quantity involving the emissivities and geometry of the bodies involved

$\sigma$  = Stefan-Boltzmann constant,  $5.67 \times 10^{-12}$  w/cm<sup>2</sup> °K<sup>4</sup>

$T_s, T_i$  = temperature of heat source and sink, respectively, °K

The heat transfer by the two mechanisms can be compared by assuming a typical spacecraft in the present simulation. Take the gas as air, with  $M = 28.9$  and  $\gamma = 1.40$ . Although  $\alpha$  is vague, a value of 0.9 (Ref. 4) looks reasonable, and  $\epsilon_{s-i} = 0.25$  would be typical for a *Ranger* vehicle.  $T_s = 300^\circ$  K and  $T_i = 80^\circ$  K are representative temperatures for a spacecraft in a space simulation. The heat transfer rates are compared in Table B-1. It is apparent that at  $10^{-6}$  mm Hg it is safe to say that there is no thermal conduction through the gas. Inside the spacecraft, smaller temperature differences and higher values for  $\epsilon$  also make this a valid criteria.

Table B-1. Comparison of radiative and conductive heat transfer in a space simulator

$P_{mm}$	$Q$ , w/cm <sup>2</sup>	$E$ , w/cm <sup>2</sup>	$Q/E$ , %
$10^{-2}$	$6 \cdot 10^{-2}$	$1.15 \cdot 10^{-2}$	520
$10^{-3}$	$6 \cdot 10^{-3}$	$1.15 \cdot 10^{-2}$	52
$10^{-4}$	$6 \cdot 10^{-4}$	$1.15 \cdot 10^{-2}$	5.2
$10^{-5}$	$6 \cdot 10^{-5}$	$1.15 \cdot 10^{-2}$	0.52
$10^{-6}$	$6 \cdot 10^{-6}$	$1.15 \cdot 10^{-2}$	0.05

## APPENDIX C

### Temperature of a Spacecraft

The temperature of an Earth satellite has been discussed in the literature (Refs. 5, 6) and will be briefly outlined here.

The temperature of a satellite or space probe is dependent only on radiative heat transfer, since it is in contact with no other bodies or conductive atmosphere. The time rate of change of the temperature of a satellite can be expressed by the following equation.

$$\frac{dT}{dt} = \frac{\alpha_1(I_{s1} + I_{s2}) + \alpha_2 I_e + P - A\epsilon\sigma T^4}{mc} \quad (C-1)$$

$T$  = temperature

$t$  = time

$I_{s1}$  = solar power directly incident upon the satellite vehicle

$I_{s2}$  = solar power reflected to the vehicle from the Earth

$I_e$  = terrestrial power incident upon the vehicle

$\alpha_1$  = absorption of vehicle's surface to solar radiation

$\alpha_2$  = absorption of vehicle's surface to terrestrial radiation

$\epsilon$  = emittance of satellite's surface

$\sigma$  = Stefan-Boltzmann constant

$A$  = vehicle's surface area

$mc$  = vehicle's heat capacity

$P$  = power dissipated within the vehicle

The terms representing the surface integrals of the radiant flux incident upon the vehicle ( $I_s$  and  $I_e$ ) can be expressed as functions of time since they are dependent on its shape, position, and attitude; and the temperature-time history of the vehicle can be obtained by integration of Eq. (C-1). This treatment applies to the evaluation of the temperature of any body in space.

The orbit of a typical satellite, e.g., an *Explorer*, is such that it spends approximately half of each revolution in the shade of the Earth. During this time, the  $I_s$  terms are zero so the vehicle temperature oscillates between maximum and minimum equilibrium temperatures. If the

power dissipated within the satellite is negligible compared to the power transferred by radiation, as in the case of the *Explorers*, these equilibrium temperatures are:

$$T_{\max} = \left( \frac{\alpha_1(I_{s1} + I_{s2}) + \alpha_2 I_e}{\epsilon\sigma A} \right)^{1/4} \quad (C-2)$$

$$T_{\min} = \left( \frac{\alpha_2 I_e}{\epsilon\sigma A} \right)^{1/4} \quad (C-3)$$

If, as in the case of the *Explorers*, the temperature of the vehicle is not significantly different from the effective radiation temperature of the Earth (250° K) then, by Kirchoff's law:  $\alpha_1 = \epsilon$ . Evaluations of the surface characteristics of several materials have shown that the absorptions of surfaces to radiation from a black body at 250° K are only slightly different from their absorptions of radiation from a black body at 300° K. Equations (C-2) and (C-3) thus show that the satellite's equilibrium temperature in sunlight is dependent on the ratio of  $\alpha_1/\alpha_2$ , while its equilibrium temperature in the shade of the Earth is independent of its surface properties. The average temperature of the vehicle can be controlled by selecting a surface for the vehicle with a ratio of  $\alpha_1$  to  $\alpha_2$  such that the two equilibrium temperatures bracket the desired mean temperature.

A space probe, e.g., the *Ranger* or *Mariner*, is simpler to discuss in that it is always in the Sun, but more complicated in that internal power is significantly large and varies with various modes of operation. It is not the purpose of this Appendix to discuss the equilibrium temperature thoroughly, but rather to indicate the factors which affect it; in particular, those factors which must be considered in the design of a space simulator, namely, the absorbed solar energy.

The absorbed solar energy is given by:  $I = \alpha_1 I_s$  per unit area, where  $I_s$  is the solar intensity and  $\alpha_1$  is the solar absorption of a surface.  $\alpha_1$  is obtained in the following manner: Let a surface whose reflectance as a function of wavelength,  $r_\lambda$  is known (this can be measured in a number of ways) be irradiated by sunlight whose spectral intensity distribution is given by  $S_\lambda$ . The incident energy is

$$\int_R S_\lambda d\lambda$$

and the reflected energy is

$$\int_R r_\lambda S_\lambda d\lambda$$

so the solar reflectance is:

$$r_s = \frac{\int r_\lambda S_\lambda d\lambda}{\int S_\lambda d\lambda}$$

For opaque surfaces, the solar absorption is:

$$\alpha = 1 - r_s = \frac{\int (1 - r_\lambda) S_\lambda d\lambda}{\int S_\lambda d\lambda}$$

(The product  $r_\lambda S_\lambda$  is not in general an analytical quantity; it is found by plotting curves point-by-point and measuring their areas with a planimeter.) The emittance,  $\epsilon$ , is obtained in an analogous manner using a black body distribution at the temperature of the spacecraft. Again, the purpose of this Appendix is not to treat the calculation of surface properties extensively but rather to indicate the factors; viz., the spectral distribution of the radiation source, which must be considered in the design of a space simulator.

## APPENDIX D

### Measurement of Spatial Intensity Distribution

This work was performed to aid in the selection of an optical system to use on the solar simulator and later in the design verification of two optical systems which were tried.

The first measurements were made of the bare carbon-arc lamp with an Eppley thermopile in conjunction with an L & N potentiometer. The thermopile was mounted on a track which was bent into an arc of a circle, the second focus of the lamp being at the center of the circle. The rail could be pivoted about in a plane normal to the lamp axis so that the entire illumination field could be measured. The thermopile was kept at constant temperature by circulating water through its jacket.

This work was repeated twice, at later dates, to verify the design of two proposed optical systems. The second time this work was performed was in evaluating the "prismatic" optical system, and the physical configuration and procedure were as shown in Fig. D-1.

The third time this work was performed was in evaluating the long focal length optical system, with several modifications to the physical configuration and procedure. Because of unfavorable constraints imposed by the peculiar radius of the curved track, and the delay in

obtaining another, much of the later work was done with a straight track by making a cosine and distance correction so that the data would be comparable with previous work performed with a curved track. Another change in equipment and procedure was to use a solar cell in place of the thermopile, recording its output with a recording potentiometer. The thermopile, with its unsealed window, had shown fluctuations resulting from room air currents on the junction. The recording feature was necessary because the solar cell did not have the inherent flicker-averaging characteristic the thermopile did, but a recording for a short interval, say thirty seconds, provided the desired averaging.

While doing the final design and design verification work on the optical system which was finally used in the solar simulator, the geometry of the detector rack was refined so that the physical configuration was identical to that of the space simulator. Referring back to Section III B, the three parameters—lamp-to-spacecraft distance, angle between lamp axis and spacecraft surface, and axis-spacecraft intersection point—were all represented in the physical configuration, as was a chamber window. Since the detector was always parallel to the plane representing the spacecraft, all intensity readings are normal components of the intensity, or effective intensity. Figure D-2 illustrates the configuration.

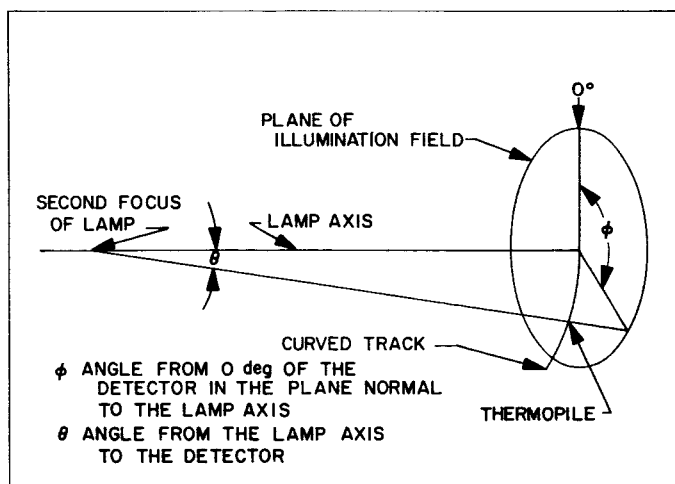


Fig. D-1. Position of detector for spatial intensity measurements

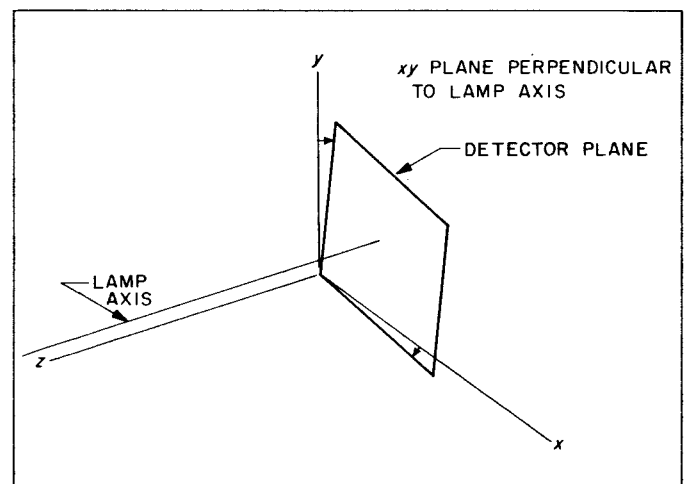


Fig. D-2. Detector plane in spacecraft orientation

## APPENDIX E

## Measurement of Radiant Power Output

The power measuring device was a very simple calorimeter adapted from other radiometers described in the literature (Ref. 7). It consists of a massive aluminum body with a tapered hole in it. The walls are anodized black within the cavity and the outside is insulated by a glasswool and aluminum foil blanket. The body is suspended by four piano wires,  $0.026 \times 10$  inches. On the basis of the low reflectance (about 7%) (Ref. 7) and the multiple reflections, the emissivity of the cavity was assumed to be unity. A copper-constantan thermocouple was placed within the body about one inch behind the cavity. This was read on an L & N potentiometer using ice water for the cold junction.

In practice, the radiant energy was allowed to enter the cone for a fixed time interval, then it was shut off and the cavity covered with an insulating blanket. The body temperature would be raised because of the addition of the radiant energy, requiring several minutes to come to equilibrium. Power data was obtained from the energy necessary for this temperature change and the time interval during which energy was absorbed by the calorimeter. The results of this test are presented in Section III E.

The power figures were derived in the following way. If a quantity of energy,  $\Delta E$ , is added to a body of a given heat capacity,  $mc$ , and is totally absorbed, then the change in temperature is  $\Delta T = \Delta E/mc$ . Rearranging and dividing by a time interval,  $\Delta t$ , gives:

$$\text{Power} = \frac{\Delta E}{\Delta t} = \frac{\Delta T}{\Delta t} mc$$

where  $mc = 1.273 \times 10^4$  w sec/deg.

Table E-1 presents a sample calculation of arc-lamp power for a typical situation.

The purpose of apertures in the solar simulator would be to regulate the intensity of the lamp radiation; hence, they were placed at the second focus of the ellipsoidal (cross-over point in the beam) where they acted as aperture stops. The cavity was placed as close to this aperture as possible, so that the diverging beam could all fall within the cavity opening. There was just enough clearance to place the aforementioned insulating blanket over the cavity during temperature stabilization. The

Table E-1. A Sample calculation of arc-lamp power for a typical situation

Thermocouple		Temperature		$\Delta T$	$\frac{\Delta T}{\Delta t}$	Power, w	$\delta$	$\delta^2$
Initial	Final	Initial	Final					
.69	.82	17.6	20.8	3.2	0.080	1020	-13	169
.82	.95	20.6	24.1	3.3	0.0825	1052	+19	361
.95	1.09	24.1	27.5	3.4	0.085	1085	+52	2704
1.09	1.21	27.5	30.5	3.0	0.075	956	-77	5929
1.21	1.345	30.5	33.8	3.3	0.0825	1052	+19	361
Average power = 1033 watts								
$\sigma = 49$								

mirror position was set with the arc at the mirror focus for all measurements, and only the mirror surface and aperture size were changed.

Three side effects investigated were: (a) the length of the time interval; (b) the initial temperature of the body calorimeter; and (c) the effect of arc-lamp feed rate.

The effects of radiation pulse duration were investigated to determine the minimum duration that the arc lamp could be on, and still give consistent results. Table E-2 gives wattage values measured using several different pulse durations.

Table E-2. Wattage values using several different pulse durations

$\Delta t$ , sec	Power, w
10	2420
20	1630
25	1590
50	1630
100	1680

The 20-sec interval was the shortest one which gave consistent results, and this corresponds to a temperature change of 2 to 3° C. Therefore, by using different size apertures, the time interval was adjusted to give about the same temperature change.

The effects of initial temperature were investigated to determine how many consecutive measurements could be made without cooling the calorimeter down to near room temperature. Table E-3 records two sets of consecutive measurements, the initial temperature for each measurement being the same as the final temperature for the preceding measurement. The time intervals are 100 sec and 20 sec, corresponding to a temperature change of about 13°C and 2½°C, respectively.

**Table E-3. Effect on measured wattage values of high initial calorimeter temperature**

$\Delta t = 100 \text{ sec.}$		$\Delta t = 20 \text{ sec.}$	
Run	Power, w	Run	Power, w
1	1720	1	1580
2	1650	2	1730
3	1580	3	1630
4	1570	4	1560
Average = 1630 $\sigma = 92$		Average = 1626 $\sigma = 66$	

Note that the elevated final temperature caused a consistent decrease in readings for the long interval while the fluctuations of the other set are random. Although the averages are nearly the same, the longer interval gave a larger  $\sigma$ , so it was decided to limit the total temperature rise to that due to five consecutive runs at the shortest possible interval.

Before it was learned that the arc current was not adjustable, data on power as a function of feed rate was taken (see Table E-4) using a 2½ in. aperture and a  $\Delta t$  of 20 sec. The table is presented here only as a matter of interest.

Two sets of data were taken using the original lamp, first with a front-surface mirror and then with a back-surface mirror. The results appear in Table E-5. The front-surface mirror yields a power increase of 32% over the back-surface mirror. Since two different mirrors were

**Table E-4. Lamp power output as a function of feed rate and current**

Feed rate, in./hr	Current, amps	Power, w
40	135-140	1920
45	140-145	2000
50	145-150	2070
55	150-155	2140

used it is difficult to say whether any of this change could be due to differences in the mirror shapes. It is reasonable to assume that the differences are due primarily to the surfacing, since the lamp manufacturer deliberately used a rear-surface mirror to eliminate UV and IR energy from the beam.

**Table E-5. Power output from front- and rear-surface mirrors**

Mirror	Power, w	$\sigma$
Front surface	2140	86
Rear surface	1625	70

There are three possible sources of errors. The first is that due to rounding off figures when extrapolating a temperature versus e.m.f. table, although this should be minimized by the multiple readings. The second is that due to unexplainable differences between various lamps. Measurements taken on the original lamp were repeated on a second lamp, with a sizeable difference. The wattages through 2½-in. apertures were 2140 and 1780 watts for the original and the second lamp respectively. Some discrepancies in the mirrors may have caused the difference. All other parameters remained unchanged between the two tests. (This points up the necessity for intensity monitoring during environmental testing.) The third source of error lies in assuming that the cavity emissivity is unity. With the largest aperture, a small amount of light struck the face of the calorimeter. Any error here, though, is on the safe side. That is, the figures are too low, if anything.

## APPENDIX F

## Measurement of Spectral Intensity Distribution

The spectral intensity distribution of an unknown radiation source can be measured by comparing it spectrally with a source whose spectral distribution is known. This comparison is accomplished by means of a spectroradiometer, the block diagram of which is shown in Fig. F-1. The symbols used in Fig. F-1 are as follows:

$I(\lambda)$  = spectral intensity distribution of radiation source

$A(\lambda)$  = percent transmission of a radiation attenuator placed in the optical path

$E(\lambda)$  = percent transmission of entrance optics

$M(\lambda, S)$  = percent transmission of monochromator, where  $S$  is the mechanical slit width

$D(\lambda, G)$  = Combined response of detector and amplifier, where  $G$  is an amplifier gain setting

$V$  = meter reading, which is a function of all previous qualities

To distinguish between events connected with the unknown source and the calibrated source, assign the subscripts  $u$  and  $s$ , respectively. The calibrated radiation source is a tungsten lamp which the NBS (National Bureau of Standards) had compared with a black body. The unit actually used was a second-generation standard with a calibration from 0.25 to 2.6 microns. This range is covered by two NBS standard lamps, 0.25 to 0.75 microns and 0.55 to 2.6 microns, from which the second-generation working standard was calibrated.

An earlier model radiometer had had the capability of scanning, so that first the spectrum of the known source could be scanned, and then the unknown source. However, the problem of detector drift was very pronounced, so the present unit was designed to compare the sources at discrete wavelengths via a flip-mirror. In practice (at each wavelength), the standard is measured, then the unknown, and then the standard again. If both measurements of the standard agree, the data is assumed valid. (Short-term changes in photomultipliers due to line voltage changes are especially bothersome.)

The derivation of the spectral intensity of the unknown source at each wavelength is as follows (see Fig. F-1):

$$I_u(\lambda) \cdot A_u(\lambda) \cdot E_u(\lambda) \cdot M_u(\lambda, S_u) \cdot D_u(\lambda, G_u) = V_u$$

$$I_s(\lambda) \cdot A_s(\lambda) \cdot E_s(\lambda) \cdot M_s(\lambda, S_s) \cdot D_s(\lambda, G_s) = V_s$$

Dividing, rearranging, and dropping the wavelength argument:

$$I_u = I_s \frac{A_s \cdot E_s \cdot M_s(S_s) \cdot D_s(G_s)}{A_u \cdot E_u \cdot M_u(S_u) \cdot D_u(G_u)} \cdot \frac{V_u}{V_s}$$

The reason for the attenuators,  $A(\lambda)$ , is that often the intensity of the known and unknown will be very different; to maintain approximately equal intensities on the detector, one or the other of the beams may be attenuated. In arc lamp work, the arc light is attenuated in the UV and visible, with no attenuation of either source in the NIR, so  $A_s(\lambda) = 1$ , always, and  $A_u(\lambda)$  is generally less than unity. The entrance optics,  $E(\lambda)$ , are identical for both beams, the same mirrors being used in both cases, therefore,  $E_u(\lambda) = E_s(\lambda)$ . If the slit settings,  $S_u$  and  $S_s$ , are identical, then  $M_u(\lambda, S_u) = M_s(\lambda, S_s) =$

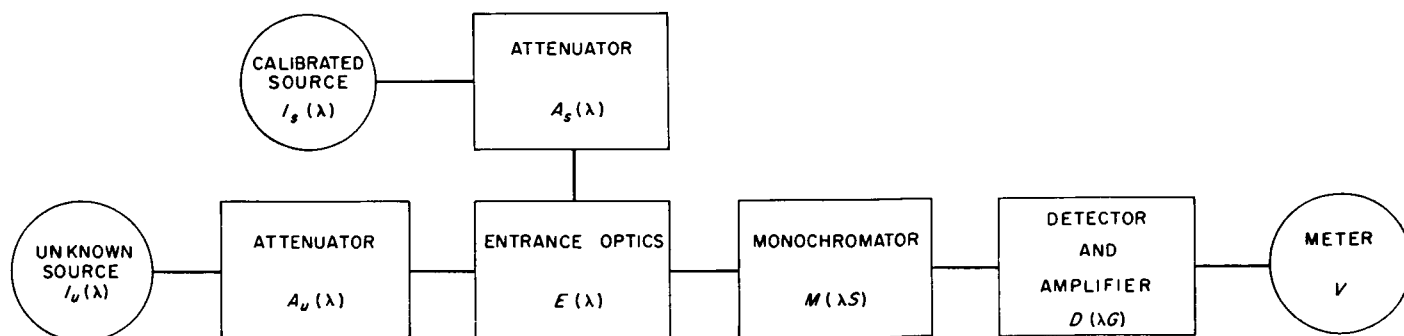


Fig. F-1. Block diagram of a spectroradiometer

$M(\lambda, S)$ . If the gain control settings,  $G_u$  and  $G_s$ , are identical, and if the detector and amplifier are linear with signal amplitude (the detector and amplifier are reputed by their manufacturer, Perkin-Elmer, to be linear to  $\pm 1/2\%$ ), then  $D_s(\lambda, G_s) = D_u(\lambda, G_u) = D(\lambda, G)$ . With these few simplifications, the equation now reduces to:

$$I_u = I_s \cdot \frac{1}{A_u} \cdot \frac{V_u}{V_s} \text{ for each wavelength.}$$

$I_u(\lambda)$  is in relative units, even though  $I_s(\lambda)$  is in absolute units. The reason for this is that the transmittance of the transfer optics used by NBS and by JPL are not identical.  $I_u(\lambda)$  can be put in absolute units by measuring the integrated intensity, e.g., with a thermopile, and equating it to the area under the spectral distribution curve.

Figure F-2 is an optical schematic of the radiometer including the P-E Model 83 Monochromator. All mirrors are of the front-surfaced aluminized type. M1 is the flip mirror used to direct energy from either the standard lamp or the unknown source into the monochromator. Energy is directed from the flip mirror to spherical mirror M3 by way of M2. By M3, it is focused on the entrance slits, overfilling them, and is collimated by the off-axis paraboloid M4 and then refracted by prism P. Littrow mirror M5 returns the selected energy through the prism to the paraboloid. The paraboloid focuses this energy on the exit slits by means of mirror M6. Mirror M7 directs

the energy to ellipsoidal mirror M8 which focuses the energy on detector target T. Mirror M7 can be removed to allow energy to pass straight on and be focused by lens L on the photomultiplier.

Chopper C interrupts the energy at a frequency of thirteen cycles per second, providing a pulsating signal at the detector (permitting the use of an AC amplifier). The detector is a thermocouple which converts the radiant energy into an electrical impulse which is proportional to the intensity of the energy. A photomultiplier can also be used as a detector in the monochromator if the signal-to-noise level becomes too low using the thermocouple. The detector signal is amplified, rectified, filtered, and fed to a millivoltmeter. Due to the differences in intensity between the tungsten filament standard lamp and the unknown source, neutral density filters can be placed into the beam of either the standard or unknown source as attenuators. Choice of the proper value neutral-density filter makes it possible for the signal strength of the standard and unknown source to be maintained nearly equal to each other at the monochromator. Keeping the meter reading near full scale during a spectral scan is achieved by use of a gain control on the amplifier. This affects both signals equally.

Entrance and exit slits, S1 and S2 respectively, control two functions. First, they control the bandwidth of the dispersed radiation to the detector and thus determine

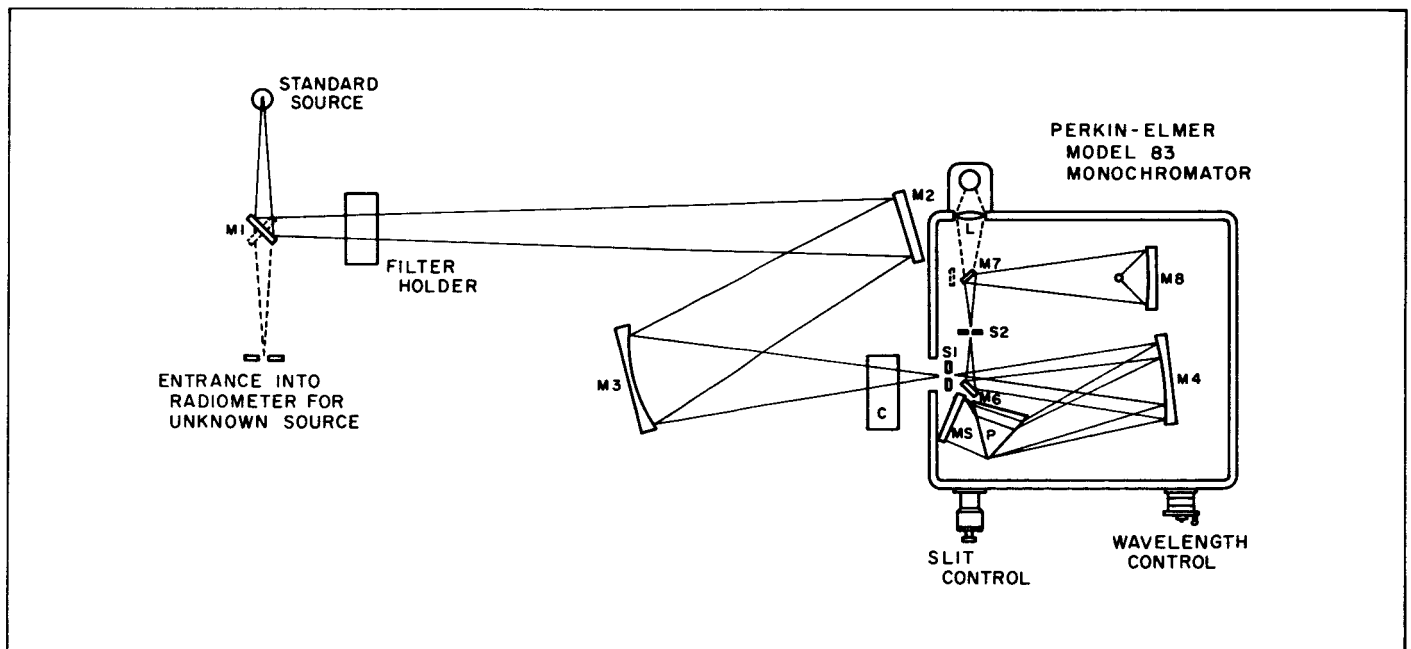


Fig. F-2. Schematic of spectroradiometer optical system



the spectral slit width. Secondly, they affect the energy incident on the detector. These slits are adjusted mechanically with a micrometer drive. The Littrow mirror is controlled by the wavelength micrometer. Discrete spectra are sampled by settings of the wavelength micrometer, where micrometer readings are converted by a calibration curve to wavelength values. The curve of drum turns (wavelength control) versus wavelength is derived using emission lines of a mercury lamp in the UV, visible, and NIR, and by an assortment of spike filters for wavelength standards farther out in the NIR. The Hg green line is used daily to check the wavelength-micrometer relationship. The transmissions of the attenuators (neutral density filters) are periodically measured in a P-E Model 4000-A double-beam ratio-recording spectrophotometer (transmission accuracy =  $\pm 1/2\%$ , according to the manufacturer).

Although there are numerous sources of error, many of them can be neglected when compared with others. The detector and amplifier, said to be linear within  $\pm 1/2\%$ , are assumed linear since the attenuators maintain the two beams well within an order of magnitude of each other. The standard lamp is assumed to be operating at the same current at which NBS operated it because our spectral distribution data is in relative units and a slight current error would not change the shape of the curve. For the same reason, the sharpness of focusing is unimportant. Because the two beams are measured very close in time, detector drift is eliminated as an error.

The largest error source is the attenuator. The attenuator consists of 1 to 5 neutral density filters placed  $1/4$  inch apart. These filters are partially reflecting, so multiple reflections can occur inside the attenuator, and near the center of the beam (where the light is reasonably parallel) unanalyzable phenomena may take place. In addition, each filter has an uncertainty, and these uncertainties compound for filters in series. The transmittance of the series of filters cannot be measured because it is so small, each individual filter yielding 10 to 50% transmission. The filters cannot be staggered, because it is doubtful whether the spectrophotometer could measure transmittance accurately if the substrate

is canted, due to beam displacement. It is possible to measure the compound transmittance while the attenuator is on the spectroradiometer by means of a black body at two widely differing temperatures. (The ratio of the two black-body emissions at some wavelength will be approximately the reciprocal of the compound transmittance.) Although this has not been done it is estimated that as much as 15% error may arise from the attenuator.

A second major error source is that due to wavelength errors, particularly on the short wavelength side of the distribution curve, where it is very steep. This is offset somewhat because in this neighborhood the prism has more dispersion, so wavelengths can be set more accurately. Both things considered, it is estimated that no more than 5% error arises from wavelength uncertainties.

The third error source is due to an uncertain spectral slit width. The data on spectral slit width versus mechanical slit width is based on a representative prism, ignoring any effect from single-slit diffraction, and assuming minimum deviation conditions at the prism. When one counts the photons within a finite spectral window centered at some wavelength, and then moves on to the next wavelength to count, he must be certain that the windows do not overlap, or he will count the same photons twice (figuratively speaking). This would result in intensity data that is too high. This effect is most pronounced in the NIR where the poor dispersion of a quartz prism results in unusually wide spectral windows. This is avoided by using the narrowest slits possible and taking data at wavelengths separated by at least two spectral window widths. On the other hand, one might use such widely spread spectral windows that he could miss much of the line structure. This is most pronounced in the UV where the high dispersion of quartz results in very narrow windows. (With a continuous spectra this is not an error.) If one suspects that emission lines are present, then these are the wavelengths at which to take measurements, provided they are not so close that the spectral windows could overlap. By proper recognition of the problem, the errors associated with spectral slit width are reduced to values which are small compared with attenuator errors.

## APPENDIX G

### Design of a Projection-Type Optical System for the Solar Simulator

This Appendix covers the design of a projection-type optical system by use of thin-lens formulae. The interrelation between optical system and irradiant intensity is shown. Because it was desirable to maintain round-the-clock operation by having only one lamp at a time shut down for servicing, it was necessary that the radiation pattern of each lamp completely cover the spacecraft.

Figure G-1 shows the simulator chamber and the entrance ports, whose location was governed by physical constraints and whose diameter was governed by window thickness constraints. The envelope of a beam which just fits through the window and just covers the spacecraft is shown, and this envelope is the minimum cone of radiation which is acceptable. However, the radiation on the upper surface of the spacecraft is the most important, so

the envelope of the beam which illuminates it is also shown. The extreme rays of this beam strike the spacecraft surface at angles of 34 deg and 4 deg. Within this cone, the effective intensity of each ray is proportional to the cosine of the angle (Lambert's law) and to the inverse square of the distance from the fireball image. Since the inverse square of the distance is proportional to the square of the cosine, the intensity is proportional to the cube of the cosine of the angle between the ray and the surface:

$$I \propto \cos^3 \theta$$

where

$$\bar{\theta} = \cos^{-1} \left[ \left( \overline{\cos^3 \theta} \right)^{1/3} \right]$$

$\bar{\theta}$  is the average value of  $\theta$ .

$$\overline{\cos^3 \theta} = \frac{\int \cos^3 \theta d\theta}{\theta_{\max} - \theta_{\min}}$$

So, for  $\theta_{\min} = 4$  deg and  $\theta_{\max} = 34$  deg,

$$\bar{\theta} = 22 \text{ deg}$$

This means that the lamp axis should strike the spacecraft surface at an angle of 22 deg to have the most uniform distribution over the upper surface of the spacecraft. (Note: Because of symmetry, the problem is only two dimensional.) The ray which strikes the spacecraft at 22 deg is shown; it is 77 in. long, and a pattern 31 in. in radius (in the plane normal to the ray) is needed to fill the minimum envelope.

At the point where each lamp axis strikes the spacecraft (during two-lamp operation) the effective radiant intensity of each must be one half the solar constant, or 68 mw/cm<sup>2</sup>. The lamp is at an angle of 22 deg, so the power from each lamp must be 68/cos 22 deg or 73.5 mw/cm<sup>2</sup> over the entire 31-in. radius plane. The total radiant output of the lamp must therefore be 73.5 mw/cm<sup>2</sup> times the area of the 31-in. radius pattern, or 1390 w/lamp. Allowing for a 15% loss because of the optics and window will require 1630 w/lamp. The data presented in Section III E indicate that a 2½-in. aperture would provide a satisfactory safety margin.

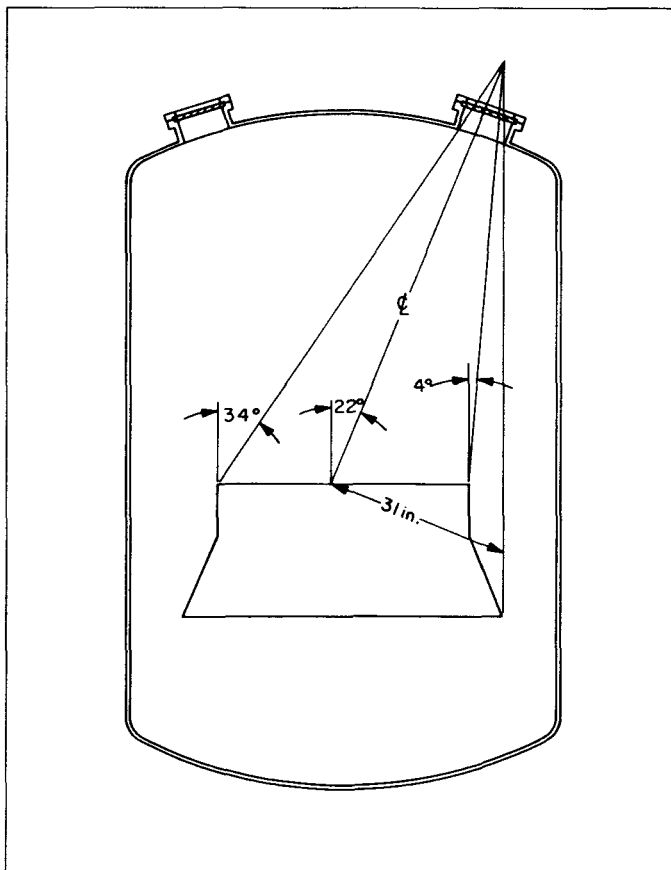


Fig. G-1. Light pattern on spacecraft in 6-ft solar simulator

Now, an optical system is needed which will magnify the 2½-inch portion of the fireball and image it 62 inches in diameter on a plane 77 inches distant.

From the laws of optics for thin lenses:

$$\text{Magnification} = \frac{s'}{s} = \frac{y'}{y}$$

$$\frac{1}{F} = \frac{1}{s} + \frac{1}{s'}$$

where

$s$  = distance from fireball to lens

$y$  = diameter of fireball

$s'$  = distance from lens to plane

$y'$  = diameter of image on plane

$F$  = focal length of lens

From the preceding discussion:

$$\text{Magnification} = \frac{62}{2\frac{1}{2}} = 24.8 = \frac{s'}{s}$$

and

$$s + s' = 77$$

therefore

$$s = 2.98 \text{ inches}$$

The necessary lens is:

$$F = \frac{ss'}{s + s'} = 2.86 \text{ inches}$$

The radiation leaving the aperture will be in a cone of 16 deg half-angle (from the geometry of the lamp proper), and so when the beam strikes the lens, it will be  $2.5 + (2 \times 2.98 \tan 16 \text{ deg})$  or 4.2 inches. It can be shown from the "lens maker's formula" that for a refractive index of 1.5, the radius of curvature,  $r$ , for such an equiconvex lens would be:

$$r = 2f(n - 1) = 2.86 \text{ inches}$$

Obviously, only a Fresnel lens could be used. Although it is possible to obtain reasonable patterns experimentally, these can't be predicted by the thin-lens formula used here. But, this system is impractical for another reason. The ellipsoidal mirror in the lamphouse is a magnifier itself, with a magnification of 6.5, to be exact. In the lamp, the arc position is stabilized by a servo system, but only to approximately  $\pm 1/32$  in., which means that the fireball image moves by  $6.5 \times 1/32$  or  $\pm 0.2$  inches. Comparing this with  $s$ , (2.98 inches), and  $F$ , (2.86 inches), it is easily seen that the lamp cannot be kept in focus, hence severe intensity variations occur. (Note: It must be pointed out that in theater use this would not be a bother as a relatively long  $s$  and  $F$  would be used.)

## APPENDIX H

### Design of Long-Focal-Length-Lens Optical System and Sunflower

This Appendix covers the design of an optical system using a long focal length lens to image the lamphouse mirror on the spacecraft. The design of a device for flattening the spatial distribution, a sunflower, is also covered. This design work was actually carried out by the authors and the system has been fabricated and used extensively. In some instances, due to physical restraints, design conditions were compromised. For example, although the lamp axis should strike the spacecraft at an angle of 22 deg (see Appendix G), this was not possible; the axis actually hit an angle of 18 deg.

As before, the basis of this system would be for each lamp to illuminate the entire spacecraft completely, so that continuous operation would be possible. Because physical constraints (guide rails and plumbing for the vacuum chamber) necessitated having the lamp axis strike 4 in. off center (at an angle of 18 deg), a 46-in. diameter (in the plane normal to the axis) would be needed to completely cover the spacecraft. The distance from lamp face to spacecraft (i.e., intersection point of lamp axis and spacecraft) was 78 in.; this dimension was imposed by physical constraints. The distance from the mirror to the face of the lamphouse measured 34.6 in. From the laws of thin-lens optics:

$$\text{Magnification} = \frac{S'}{S} = \frac{Y'}{Y}$$

$$\frac{1}{F} = \frac{1}{S} + \frac{1}{S'}$$

where

$S$  = distance from mirror (object) to lens

$Y$  = diameter of mirror (object) = 21 in.

$S'$  = distance from lens to spacecraft (image)

$Y'$  = diameter of spacecraft (image) = 46 in.

$F$  = focal length of lens

From the preceding discussion:

$$\text{Magnification} = \frac{46}{21} = 2.19 = \frac{S'}{S}$$

and

$$S + S' = 34.6 + 78 = 113 \text{ inches}$$

therefore

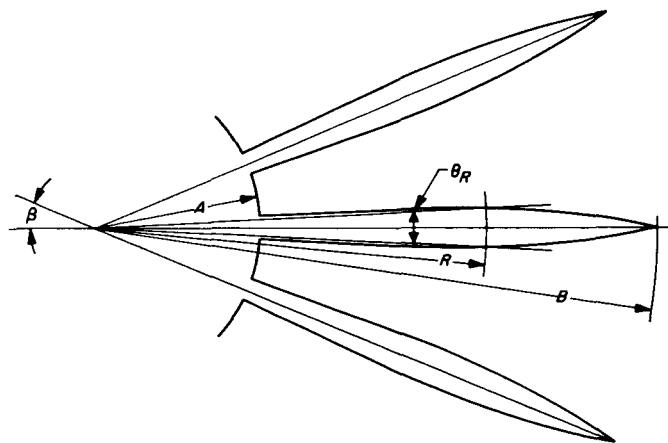
$$S = 35.4 \text{ inches}$$

If  $S$  were shorter, the pattern would over-cover the spacecraft. Since this would result in greater uniformity and it would make a simpler mechanical situation, the lens was mounted at the face of the lamphouse,  $S = 34.6$  in.

$$F = \frac{SS'}{S + S'} = \frac{34.6 \cdot 78}{113} = 23.9 \cong 24 \text{ inches}$$

The lens diameter was 4 in., a dimension obtained by measurement of beam diameter at the lamphouse face. No apertures are considered because another scheme for controlling energy was to be used.

The spatial distribution of an arc lamp with the long focal length lens is given in Fig. 8 of the report proper. The distribution is characterized by having ample power in the center with a steep fall-off toward the edges and a shadow in the center (because of the hole in the lamp mirror). A device could be placed in the beam, far enough from the mirror so that it would be out of focus, which would selectively attenuate the beam; heaviest attenuation at the center, little or none at the edges. Such a device, called a sunflower, is shown in Fig. H-1. The percent transmission, as a function of radius, is given



$\beta$  = ANGLE BETWEEN BLADES

$A$  = RADIUS OF HUB

$B$  = RADIUS AT WHICH TRANSMITTANCE IS 100%

$R$  = RADIAL DISTANCE FROM CENTER

$\theta_R$  = ANGULAR WIDTH OF BLADE AT  $R$

Fig. H-1. Blades typical of those used on the sunflower

by the ratio of open area to total area for the annulus defined by each radius.

The purpose of a sunflower is to make the transmission as a function of radius,  $T_r$ , be the inverse of the spatial distribution, but only over the portion of the distribution to be attenuated. Figure H-2 is a sample spatial intensity distribution for which a sunflower to attenuate the center to 0.8 solar constants will be designed.

For convenience, the ordinate scale reads both solar constants and transmission, 1.0 being 100% transmission. The product of the two curves,  $I_r$  and  $T_r$ , equals 0.8 solar constants. (An earlier designed sunflower assumed that  $I_r$  was a straight line, so that  $T_r$  was analytical, but this caused peculiarities near the extremes of the resultant spatial distribution.) By geometry, radial distance on the sunflower is related to radial distance in the spatial distribution. For the pattern past the radius where  $I_r = 0.8$  solar constants, the sunflower could do nothing. However, introducing a piece of ground Vycor into the beam filled it in somewhat. [The reason for the high intensity (0.8 solar constants) from each lamp is that scattering caused by the ground Vycor cut the irradiation level down to about half.]

The foregoing has been very general; only a spatial distribution curve and a sunflower for it have been considered. In reality, the arc lamp has a spatial distribution which is not only radially unsymmetric, but rotationally as well, due to the hole in the lamp mirror being cut off-center. Further, the lamp axis is not normal to the spacecraft, so there is a variation rotationally due to differences in distance and, so far as the spacecraft thermal input is concerned, the angle at which each ray strikes the surface (Lambert's law). This rotational dissymmetry must also be removed by the sunflower by making it rotationally unsymmetrical. The spatial distribution curves to which the sunflowers were designed were obtained by placing the lamp and the measuring device in an exact space simulator configuration (see Appendix D). In this way, all causes of the rotational effects were included in the design. Each blade of the sunflower was individually designed, using the spatial distribution of the corresponding location on the spacecraft.

The larger the number of blades, the better that their shadow diffused. (Although the sunflower was not in focus, blurs of the blades could be seen if the ground

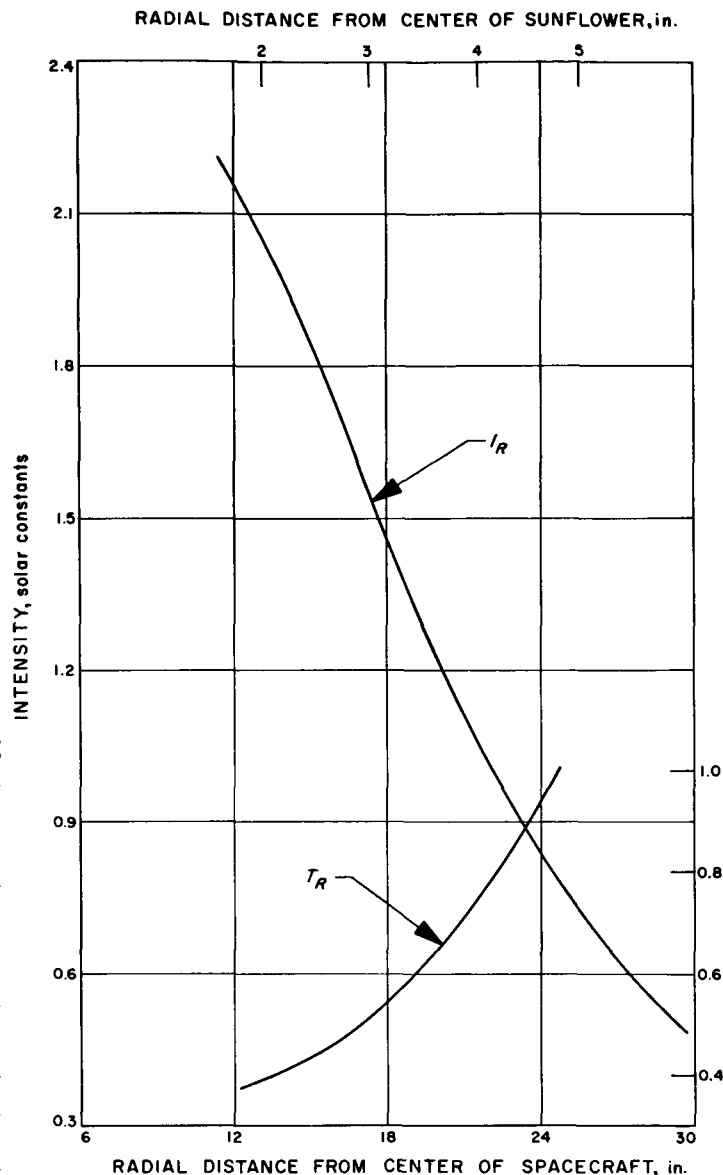


Fig. H-2. Typical spatial distribution ( $I_r$ ) and its transmittance curve ( $T_r$ )

Vycor wasn't used.) The final design used 32 blades, that number being the maximum commensurate with fabrication ease. The sunflowers were cut from a sheet of 1/4-in. copper, so that a cooling coil could be attached to the hub. However, the temperature in use was only 250°F, so the cooling line was never attached. The blades oxidized to a dull black in use (this was their condition when the 250°F temperature was measured). No erosion of the blades has taken place in over half a year of service.

## REFERENCES

1. Yarwood, J., *High Vacuum Technique: Theory, Practice, Industrial Applications, and Properties of Materials*, 3rd ed. rev., John Wiley and Sons, Inc., New York, 1955, p. 1.
2. Dushman, S. D., *Scientific Foundations of Vacuum Technique*, John Wiley and Sons, Inc., New York, 1949, pp. 52-53.
3. Brown, A. I. and Marco, S. M., *Introduction to Heat Transfer*, 3rd ed. McGraw-Hill, New York, 1958, p. 63.
4. Dushman, S. D., *Scientific Foundations of Vacuum Technique*, John Wiley and Sons, Inc., New York, 1949, Table 1-13.
5. Hibbs, A. R., *The Temperature of an Orbiting Missile*, Progress Report No. 20-294, Jet Propulsion Laboratory, Pasadena, March 28, 1956.
6. Shipley, W. S., "The Environmental Testing of Space Probes," paper delivered to the Los Angeles Chapter of the Society of Environmental Engineers, April 6, 1959.
7. Flood, W. F., "Simple Way of Measuring the Power of High-Intensity Light Beams," *Review of Scientific Instruments*, Vol. 30, No. 6, June 1959, p. 487.